Anal. Bioanal. Electrochem., Vol. 12, No. 7, 2020, 904-921

Analytical& Bioanalytical Electrochemistry

Full Paper

Corrosion Behavior of Ti/TiN Multilayer Nanostructured Coatings Applied on AISI 316L by Arc-PVD Method in the Simulated Body Fluid

Shiva Zaheri, Arash Fattah-alhosseini,* Hassan Elmkhah, Kazem Babaei, and Omid Imantalab

**Department of Materials Engineering, Bu-Ali Sina University, Hamedan 65178-38695, Iran*

*Corresponding Author, Tel.: +988138292505; Fax: +988138257400

E-Mail: a.fattah@basu.ac.ir

Received: 22 May 2020 / Received in revised form: 9 July 2020 / Accepted: 10 July 2020 / Published online: 31 July 2020

Abstract- In this investigation, Ti/TiN nanolayer and TiN single layer coatings were coated on substrate of AISI 316L stainless steel by applying physical vapor deposition (PVD) using the type of cathodic arc evaporation (CAE). The evaluation of microstructure were carried out using x-ray diffraction (XRD), nanoindentation, atomic force microscopy (AFM) as well as scanning electron microscopy (SEM). Polarization and impedance tests were utilized to study the coatings corrosion behavior in the simulated body solution (SBF) in different immersion times. Utilizing CAE technique, high density and adhesion Ti/TiN nanolayer and TiN single layer coatings were successfully made. The corrosion results showed that Ti/TiN nanolayer coating had an exceptionally high polarization resistance compared to 316L substrate and TiN single layer coating. Furthermore, the corrosion results indicated the desired corrosion behavior in the nanolayer coating towards the single layer within the SBF, as a result of the distinct layers presence resulting in a barrier against penetration of the corrosive media.

Keywords- Physical vapor deposition (PVD); Nanostructured coating; Ti/TiN; EIS; Polarization

1. INTRODUCTION

Nowadays, biomaterials are widely utilized in the field of producing implantations in human body and their most significant ones are the 316L stainless steel. These materials are mainly utilized for orthopedic and dental applications because of their low expenditure, simple production and suitable corrosion resistance. Easy surface cleaning and neutralization are the other specifications of stainless steel [1–4]. These materials work inappropriately while being exposed to long term exposure especially in corrosive surroundings, though. Reports have shown that 74 percent of these implants fracture in the cervical district on account of wear corrosion. One of the basic features of these steels is their great susceptibility to pitting corrosion. This feature makes deep cavities on the metal surface; the commencement of pitting corrosion may be on account of the reaction between an oxidizer like dissolved oxygen with chlorine ion. The oxygen presence in the cells can also begin or accelerate its primary corrosion [5]. An adhesive oxide layer covers the whole outer layer of the metal because of the chromium element presence. This oxide layer, that is called the passive layer, is formed by the reaction between oxygen and chromium [6]. Coating the implant can be a sensible solution to avoid corrosion and abrasion and to augment the pitting corrosion resistance for preventing the mentioned occurrences.

Generally, transition metal nitride coatings are widely utilized for various applications because of their hardness, friction coefficient, corrosion resistance, biocompatibility and wear resistance [7, 8]. Amid the different types of coatings, Ti/TiN multilayer coatings are being used due to high corrosion resistance, optimum wear resistance and proper biocompatibility as well as significant mechanical properties [9–11].

Amid the coating techniques, the PVD method boosts the chemical and mechanical properties of the implant material because of making a dense coating that produces coatings having high wear and corrosion resistance in relatively low production cost [12–14]. The most highly utilized method to produce thin films is PVD [15, 16]. The deposition of thin and hard coatings requires a wide range of PVD methods including magnetron sputtering, CAE and combined magnetron and arc procedures [16, 17]. As a deposition method, CAE is one of the most widely utilized ones on account of its great coating characteristics like good adhesion-to-substrate, homogeneity, high hardness and density and as a result, better properties than coatings that were produced magnetron sputtering due to the ionization rate in the arc-PVD method is much higher than that in the magnetic sputtering [18–23]. In general, CAE aids removing various kinds of coatings like metal carbides, nitrides and pure metals. The cathode ionization may be made by ions that move towards the substrate located on the negatively polarized, rotatable holder. Diverse ambiences in the chamber are applicable depending on the deposited coatings nature; inert gas-argon is required for metal coating, and nitrogen for metal nitride coating [19, 23–25].

Chenglong et al. [26] evaluated the hemocompatibility and corrosion resistance of Ti/TiN multilayer coatings on 316L using ionic plating method in the Tyrode's SBF (pH=7.4) at 37± 1 ºC. Also, Nam et al. [27] evaluated the corrosion behavior of Cr/TiN, Ti/TiN, Cr/CrN and Ti/CrN multilayered coatings on AISI 316L using CAE technique in 1 M H_2SO_4 + 2 ppm F. Recently, Andalibi Fazel et al. [18] studied the electrochemical behavior of applied TiN single layer and CrN/TiN nanoscale multilayer coatings deposited by CAE technique. Although the wear and corrosion resistance of Ti/TiN coatings have been studied, there is no systematic research on the corrosion resistance of Ti/TiN multilayer coatings applied on 316L using CAE in the simulated body fluid. Therefore, for present work, the Ti/TiN multilayer coatings first, were deposited by CAE process on 316L. Second, the corrosion resistance of coatings was investigated in the simulated body fluid (SBF) for 14 days. To reach these purposes, the potentiodynamic polarization plots for all coatings were implemented along with the electrochemical impedance spectroscopy (EIS) curves in SBF electrolyte.

2. EXPERIMENTAL PROCEDURE

Ti/TiN multilayer and TiN single layer coatings were deposited by CAE machine on AISI 316L stainless steel substrate. In this method, pure commercial titanium was utilized as the target material. The deposition and device conditions are given in Table 1. Before deposition process, the specimens surface finishing was carried out by SiC papers up to 2000 grit. Then the specimens were kept in ultrasonic bath for 15 minutes. Then, the specimens exposed in argon environment at the -800 V substrate bias voltage for ion bombardment which can improve adhesion. Argon gas was kept constant during the coating procedure, but the nitrogen gas was cut off in the deposition of the multilayer coating during deposition of the pure Ti layer and then reconnected when the TiN layer deposited.

Table 1. Coating parameters using CAE method in this study

Target material	**Titanium** 99.95 %
Working pressure (torr)	5×10^{-3}
Current of target evaporation (A)	100
Distance of target to the substrate (cm)	15
Deposition time (min)	60
Substrate rotating rate (RPM)	5
Duty cycle	50%
Coating temperature (ºC)	200

The x-ray diffraction (XRD) pattern was utilized by the Philips PW1730 diffractometer using a Cu Kα beam (wavelength equal to 1.54 angstroms) from 20 to 80 degrees of diffraction angle to identify the phases in the coated specimens. Diffraction patterns were analyzed by Xpert HighScore software. Scanning electron microscopy (SEM) of model JEOL JSM-840A and FEI ESEM QUANTA 200 were also utilized to study the surface microstructure and cross-sectional area of the coatings. NanoScope III atomic force microscopy (AFM) of model Digital Instruments, USA was used to investigate the surface roughness and the coatings structure. The scanning size was 5 μm and the scanning rate was 2.001 Hz and the data scale is 200 nm. In this investigation, devices of A Hysitron Inc. TriboScope® and 3000 N force have been used to study nanohardness of the coated specimens.

The surface grinding of the samples was carried out using SiC paper up to 5000 grit for electrochemical tests. The specimens were then washed with distilled water and quickly dried after cooling with cold air. Then they were tested. An ordinary flat cell was utilized in which the specimens were used as the working electrode (the exposed surface was 0.78 cm^2), a silver/ silver chloride electrode as the electrode of reference and platinum electrode as auxiliary electrode. The used SBF solution was provided in accordance with the Kokubo's proposed method [28]. The used compounds in order to make this solution are indicated in Table 2.

Electrochemical measurements were carried out by a μautolab potansiostat/galvanostat. Several electrochemical tests including potentiodynamic polarization and EIS have been utilized in this investigation. The potentiodynamic polarization analysis with a scanning rate of 1 mV/s began from -0.25 V to the open-circuit potential and kept on till the passive layer failure potential. EIS test was carried out in the frequency range of 100 kHz to 10 mHz.

Table 2. Values of SBF solution compositions in 1000 ml [23]

Order	Reagent	Amount
1	NaCl	8.035 (g)
2	$NaHCO_3$	0.355 (g)
3	KCl	0.225 (g)
4	$K_2HPO_4.3H_2O$	0.231 (g)
5	$MgCl_2.6H_2O$	0.311 (g)
6	1M-HCl	39 ml
7	$CaCl_2$	0.292 (g)
8	Na_2SP_4	0.072 (g)
9	Tris	6.118 (g)
10	1M-HCl	0-5 ml

3. RESULTS AND DISCUSSION

3.1. Microstructural evolutions

Fig. 1 depicts the XRD patterns of TiN and Ti/TiN coatings. According to Fig. 1, the peaks related to Ti, TiN, and Fe with the miller index of their plates are observed. The titanium and titanium nitride phase exist with the hexagonal closed packed (HCP) and the faced centerd cubic (FCC) structure, respectively by using the presented pattern in the deposited coating. The lower intensity of the multilayer peaks than that of the single layer coating attribute to the amorphous value of multilayer structure compare to that in the single layer coating [19].

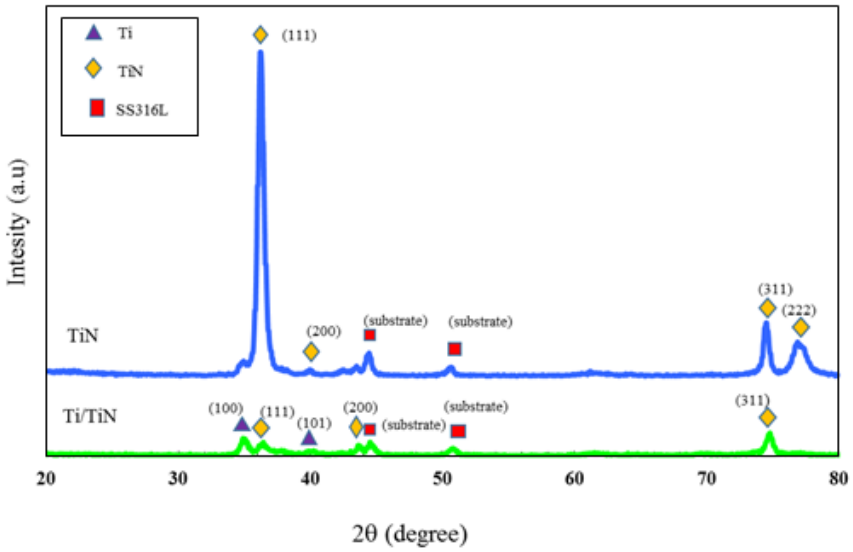

Fig. 1. XRD patterns of TiN and Ti/TiN coatings

Fig. 2 illustrate the field emission SEM (FESEM) images of cross-section of Ti/TiN multilayer and TiN single layer coatings. Equal thicknesses were observed for both coating. It should pointed out that Ti and TiN multilayer were have same thickness. Considering Fig. 2, the nanoscaled layer structure of the multilayer coating is clearly visible. According to Fig. 2, good adhesion of the coating to the substrate is obvious and the made coating is crack free. It can be said that presence of the Ti layer cause to the good adhesion in the multilayer coating [29]. The titanium layer presence between the titanium nitride layers prohibits the growth of coaxial columnar grains, which amends the coating density and augments the bond consistency of the coating [30]. This also causes the re-nucleation of titanium nitride crystal that leads to reduction of the existing defects and therefore rises the coating density. The interlayer of titanium acts as a bumper against the residual stress and declines the residual stress. On the other hand, the created stress in the coating is spread and declined among the pair of layers, which results in a higher density of structure and higher adhesion of the coating to the substrate and the layers in the multilayer coating towards the single layer coating [31–34]. Based on published scientific sources, multilayer

coatings make the residual stresses decline in the coating leading to a better adhesion of coating to the substrate [30, 35].

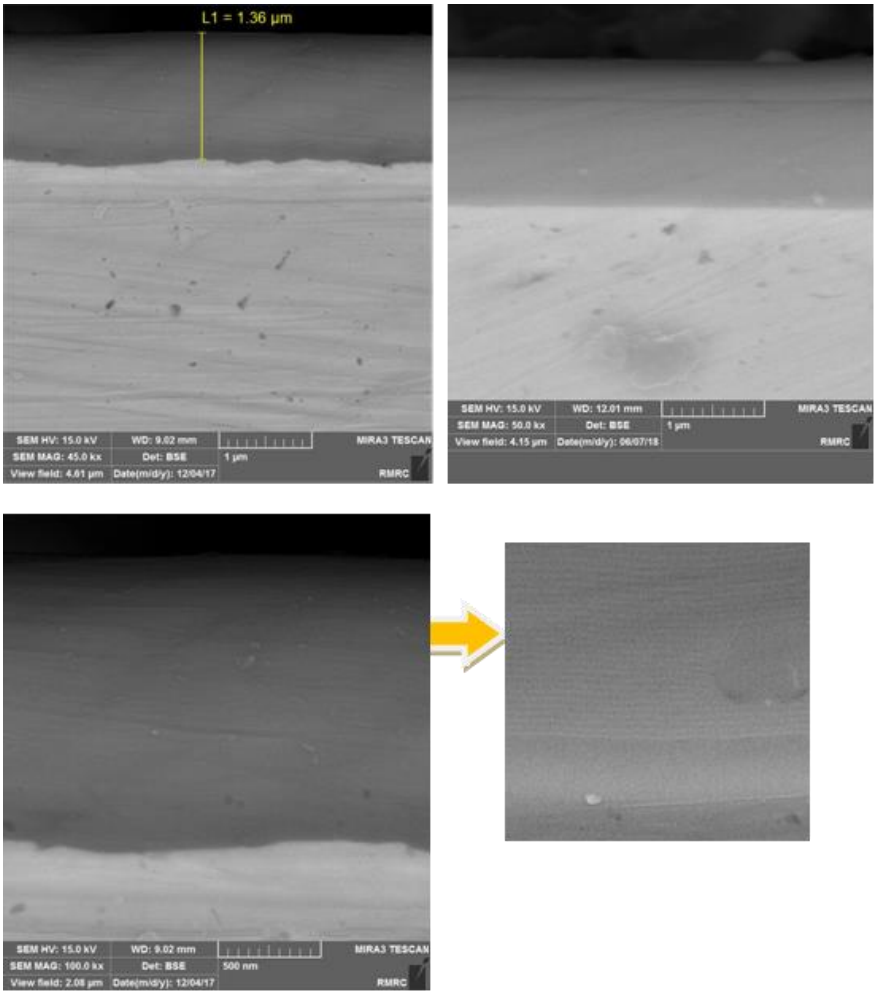

Fig. 2. (a, b) FESEM image of cross-section of Ti/TiN multilayer coating, (c) TiN single layer coating

Fig. 3 shows the SEM images of the multilayer and TiN single layer coating surfaces. Indeed, presence pin-holes and macroparticles is an inherent feature of deposited coatings using CAE method [12]. Since the surface layer of the nanostructured multilayer coating is similar to the TiN single layer coating, there are many similarities between the two parts of (a) and (b) of Fig. 3. However, the existing pin-holes in single layer coating has been fewer than that of multilayer. Having a coaxial column structure for single layer coating, more pin-holes are involved. Fig. 4 reveals the energy dispersive x-ray spectroscopy (EDS) analysis of the macroparticle in the coating. This diagram shows the composition of the macroparticles in the coating mainly include titanium and nitrogen elements.

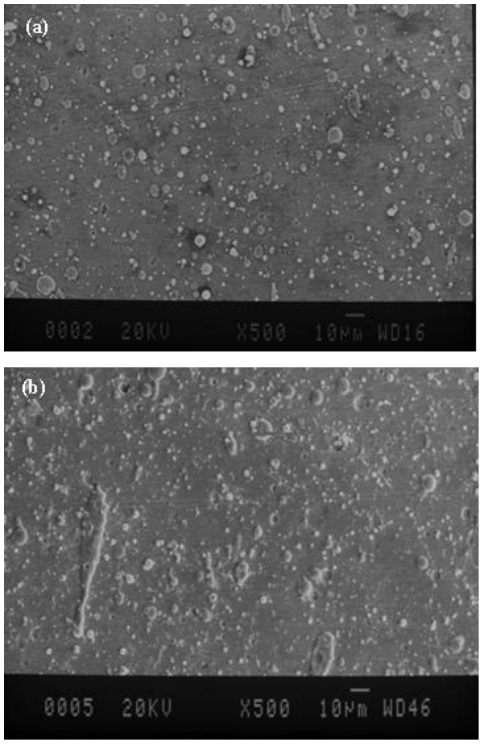

Fig. 3. SEM image of (a) Ti/TiN multilayer nanostructured coating surface, and (b) TiN single layer coating surface

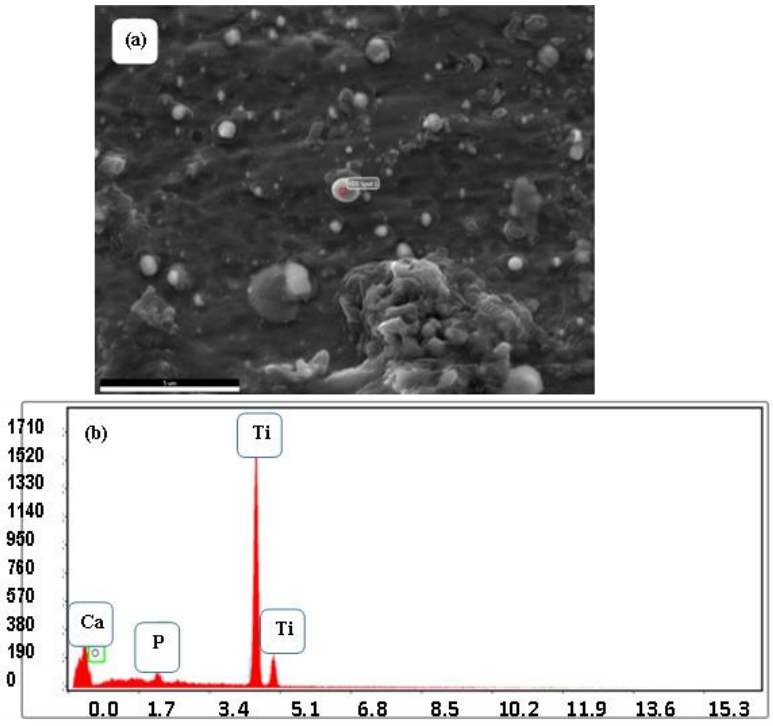

Fig. 4. (a) SEM image of the macroparticle in the coating for EDS analysis, (b) EDS analysis of the macroparticle

3.2. Roughness and mechanical evaluation

Fig. 5 illustrates image of the obtained surface roughness Ti/TiN multilayer nanostructured coating and TiN single layer coating using AFM. As can be observed, the average roughness (Ra) in the 5-µm by 5- µm area of the multilayer nanostructured coating is 40.975 nm and that of the single layer coating is 76.145 nm. The highest grain height in the multilayer coating is 368.76 nm and in the single layer coating is 431.71 nm. The small size of the macroparticles is attributed to the presence of the inter layer of pure titanium. As previously mentioned, the presence of Ti interlayer prevents the growth of co-axial columnar crystals and, on the other hand, results in the re-nucleation of titanium nitride crystals both causing greater fineness and increase the structure density in Ti/TiN multilayer nanostructured coatings. Having a smooth surface results in the formation of a homogeneous and uniform passive film that rises the corrosion resistance.

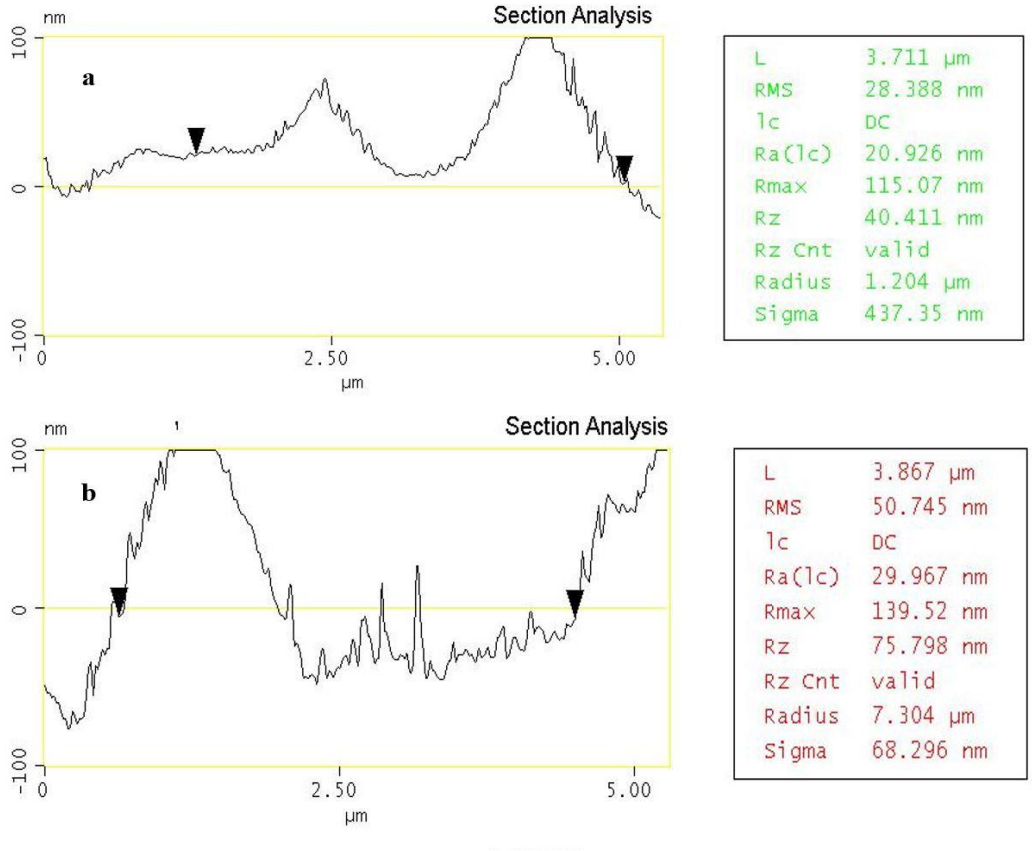

Fig. 5. Diagram of the surface roughness using AFM for (a) multilayer nanostructured Ti/TiN coating, and (b) TiN single layer coating

Fig. 6 illustrates the nanoindentation diagrams (displacement-load curves) of Ti/TiN and TiN single layer coatings. As can be seen, the maximum load for the testing is 3000 µN. The obtained data from Fig. 6 is reported in Table 3. Based on Table 3, the elastic modulus and

hardness of Ti/TiN nanostructured coating were higher than that of TiN single layer coating. According to published scientific sources, it can be said that there is no possibility for displacements moves in nanoscale-size boundaries and the interfaces between two nanolayers in multilayer coatings and as a result, displacements have been locked and causes the multilayer coating structure to be hardened. Since the structure of the multilayer coating is denser than the single layer coating and has fewer holes, it has a higher elastic modulus [36]. On the other hand, the single layer coating has more holes on account of having a coaxial columnar structure that declines the bond energy (which makes the elastic modulus to be diminished) [37].

Table 3. Obtained data from the nanoindentation test

	TiN single layer coating	Ti/TiN nanolayer coating
Hardness, H_V (GPa)	17.96	21.74
Elastic modules, E (GPa)	363.8	390.0

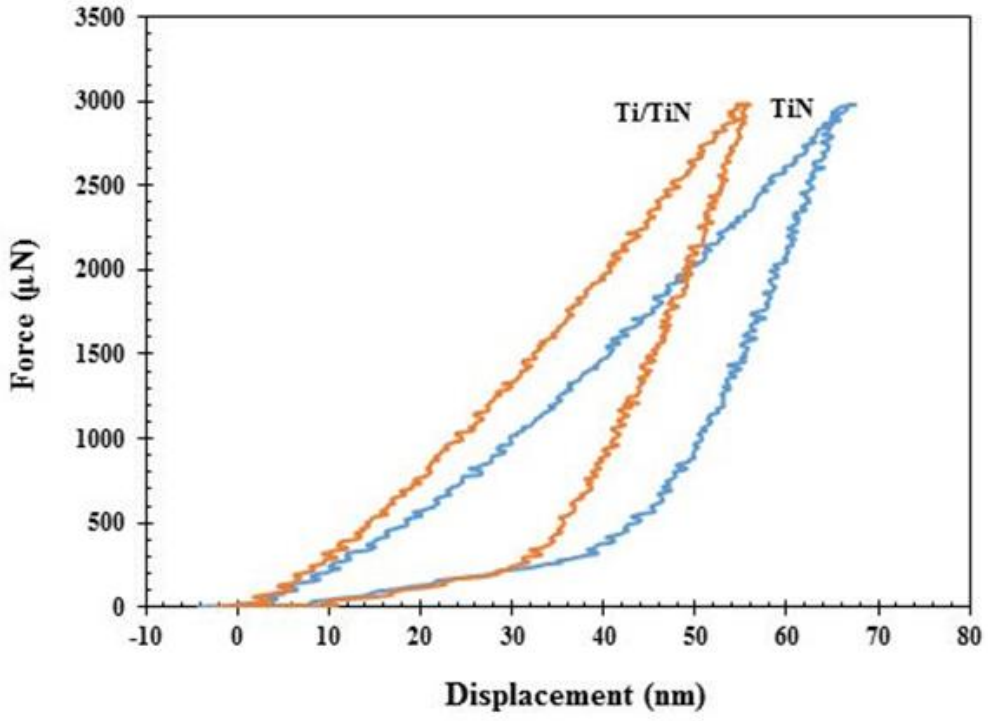

Fig. 6. Nanoindentation diagram of TiN and Ti/TiN coatings

3.3. EIS tests

Figs. 7 and 8 show the EIS plots of Ti/TiN multilayer nanostructured coating, TiN single layer coating, and 316L in SBF solution after different immersion times. Similar Bode-module plots were reported for Cr/TiN, Ti/TiN, Cr/CrN, and Ti/CrN coatings on 316L using CAE technique in 1 M H_2SO_4 + 2 ppm F [27]. As can be seen, based on the Nyquist diagrams

shown in Fig. 7, the capacitance rings corresponding to the multilayer coating are larger than that of the other studied specimens (TiN single layer and substrate) at any given time. The larger capacitance ring diameter of each specimen in the Nyquist plot is attributed to its better corrosion behavior. Also, based on the Nyquist diagrams indicated in Fig. 7, the behavior of non-ideal capacitance for all of the specimens investigated in the SBF electrolyte is obvious. According to the Bode-module diagrams shown in Fig. 8, the impedance value for the specimen having multilayer nanostructured coating is higher at low frequencies. Thus, rising the value of impedance indicates increased corrosion resistance of the coating.

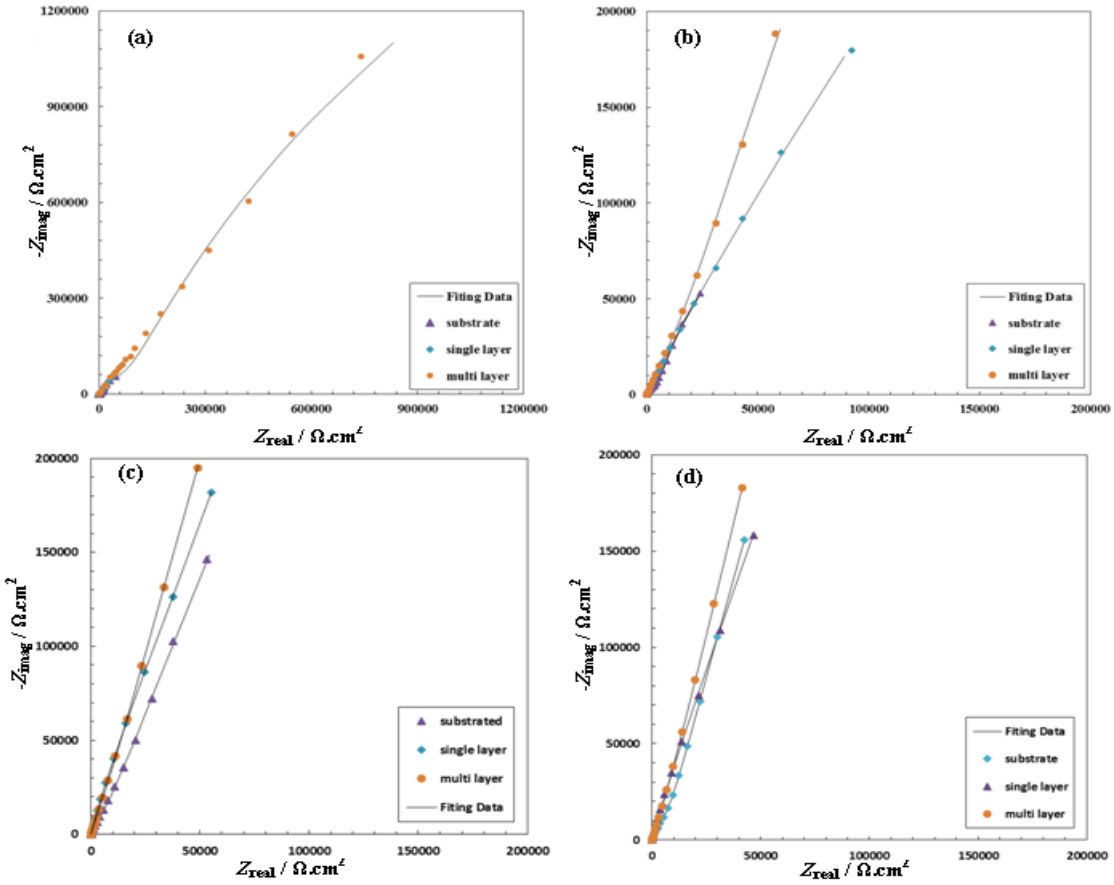

Fig. 7. Nyquist plots of nanostructured Ti/TiN coating, TiN single layer coating, and 316L stainless steel in SBF solution after different immersion times: (a) 3, (b) 24, (c) 168, and (d) 336 h

The 316L stainless steel substrate is particularly susceptible to pitting corrosion. Proteins in the body corrode the implants by augmenting the dissolution of elements like cobalt and chromium, and the presence of chromium causes the formation of Cr_2O_3 passive film. The corrosion behavior of implant has changed by applying coating and showed less sensitivity to pitting corrosion and the presence of pinholes and macroparticles on the surface of coatings are considered as an appropriate place for corrosion attacks. The pinholes act as a route for

the corrosive material penetration and the droplets and macroparticles are proper locations to commence the formation of local and pitting corrosion in the coating. These locations are fewer and on the other hand, the presence of several inter layers prevents penetration of the corrosive solution into the substrate in the multilayer coating [30].

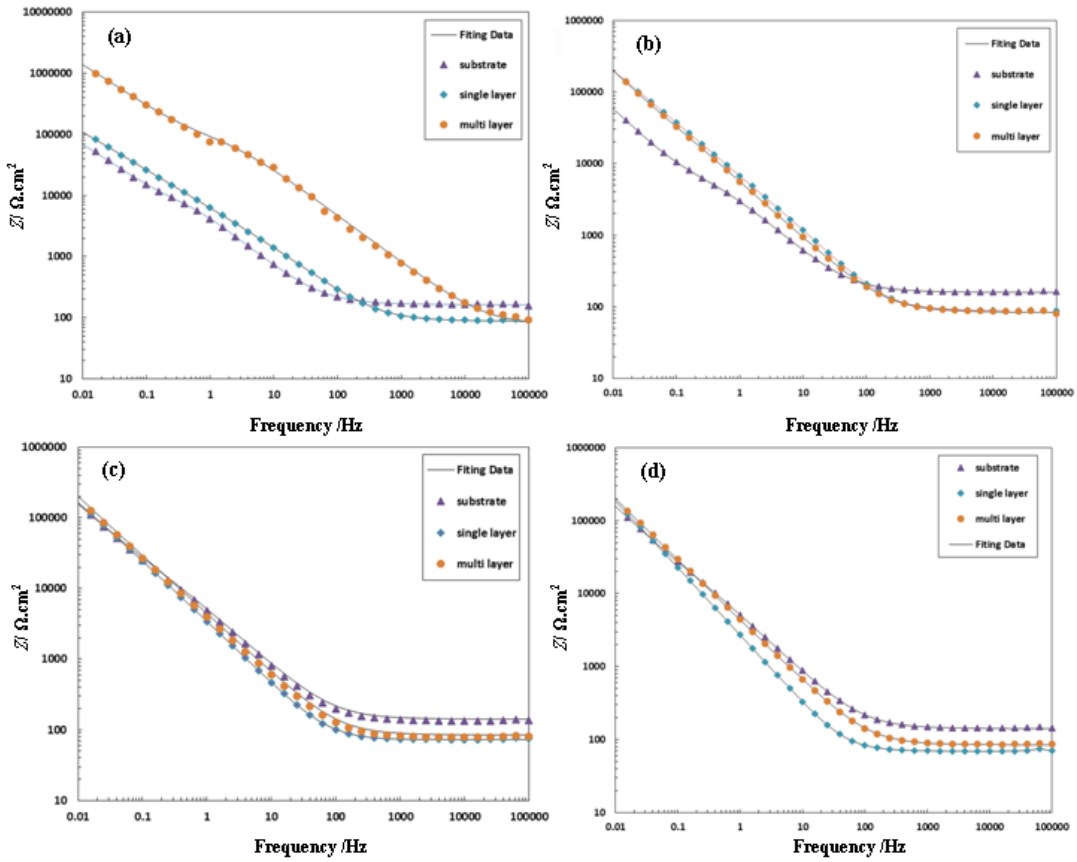

Fig. 8. Bode-module plots of nanostructured Ti/TiN coating, TiN single layer coating, and 316L stainless steel in SBF solution after different immersion times: (a) 3, (b) 24, (c) 168, and (d) 336 h

On the other hand, by the corrosive solution penetration into the pinholes, localized corrosion occurs on the surface and the upper and inter layers interact. Then it becomes suitable for galvanic corrosion because of differences in bonding energy and chemical composition of this location. Passing the time, the corrosion products fill in the pinholes and this prevents corrosion, and the corrosive solution is supposed to find another route to penetrate. As the density of the structure makes less penetration of the corrosive material into the coating, the multilayer coating has a higher density due to prevention of the coaxial columnar structure growth and helping to re-nucleation of titanium nitride crystals and fewer defects in the coating structure that this more density increases the corrosion resistance towards the single layer coating [38–41]. On the other hand, non-adhesion is the other reason to corrosion accelerating process. The adhesion of the multilayer coating is more than that of

the single layer coating, which is ascribed to the lower residual stress in the multilayer coating, therefore increases the corrosion resistance of the multilayer coating is more than the single layer coating. Surface roughness is the other effective factor on the corrosion process. As the surface roughness declines, suitable locations for corrosion attacks will diminish.

Table 4. Extracted results using the proposed equivalent circuit after immersion in SBF solution

Sample	Time of immersion (h)	R_{inner} (MΩ.cm^2)	R_{outer} (MΩ.cm^2)
316L	3	0.453	0.005
TiN		1.88	0.004
Ti/TiN		15.2	0.017
316L	24	0.525	0.006
TiN		1.52	0.006
Ti/TiN		9.87	0.018
316L	168	14.3	0.0068
TiN		8.75	0.001
Ti/TiN		23.4	0.007
316L	336	16.3	0.008
TiN		23.1	0.0009
Ti/TiN		41.8	0.146

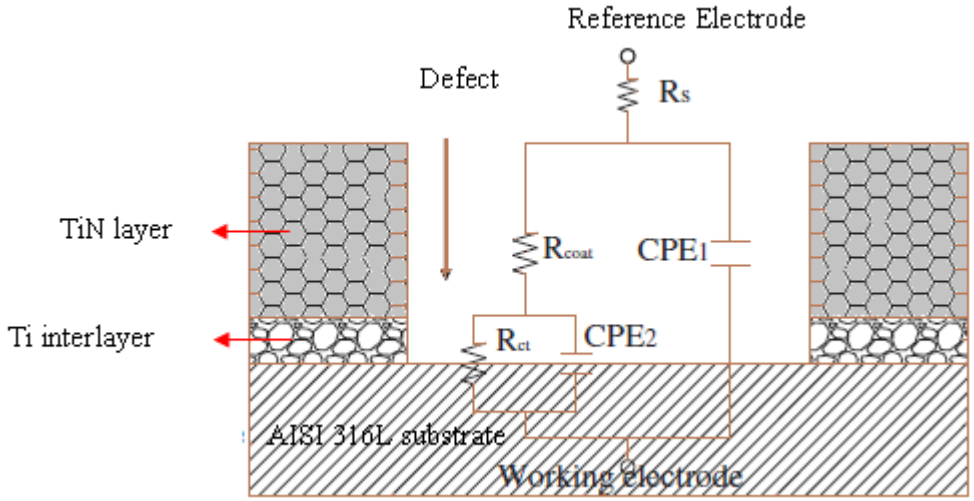

Fig. 9. Best EEC used for modeling the EIS data

Based on published sources [42, 43], the formed passive film structure applied on 316L is a dual structure with a dense Cr-rich inner film and a Fe-rich porous outer film. Therefore,

the equivalent electrical circuit (EEC) of Fig. 9 is used to simulate EIS data [27,44-46], where R_S shows the resistance of solution, CPE_1 represents the constant phase element (CPE) of the coating, R_{coat} is the resistance of coating, CPE_2 reveals the CPE of the double layer, R_{ct} represents the charge-transfer resistance. The obtained parameters from the simulation of the EIS test the experimental data (illustrated in Figs. 7 and 8) related to considered specimens in the present study has been summarized in Table 4. The results show higher polarization resistance (R_{ct} + R_{coat}) for Ti/TiN multilayer coating than TiN single layer coating and uncoated 316L substrate at any given time.

3.4. Polarization measurements

Fig. 10 depicts the polarization plots of 316L, TiN and Ti/TiN coatings in SBF solution for 336 h immersion. As can be seen, the passive behavior of all specimens is clear in the studied solution. Similar potentiodynamic polarization plots was reported for high power impulse magnetron sputtering-TiN and direct current magnetron sputtering (DCMS)-TiN coatings in 3.5% NaCl solution [10]. Coating the AISI 316L stainless steel makes corrosion current density decline. Rising corrosion potential in the multilayer coating is on account of not having adequate time to attain the solution to substrate through defects and pinholes and macroparticles in the coating, presenting good adhesion between the coating and the substrate [47]. Table 5 summarizes the obtained data from Fig. 10.

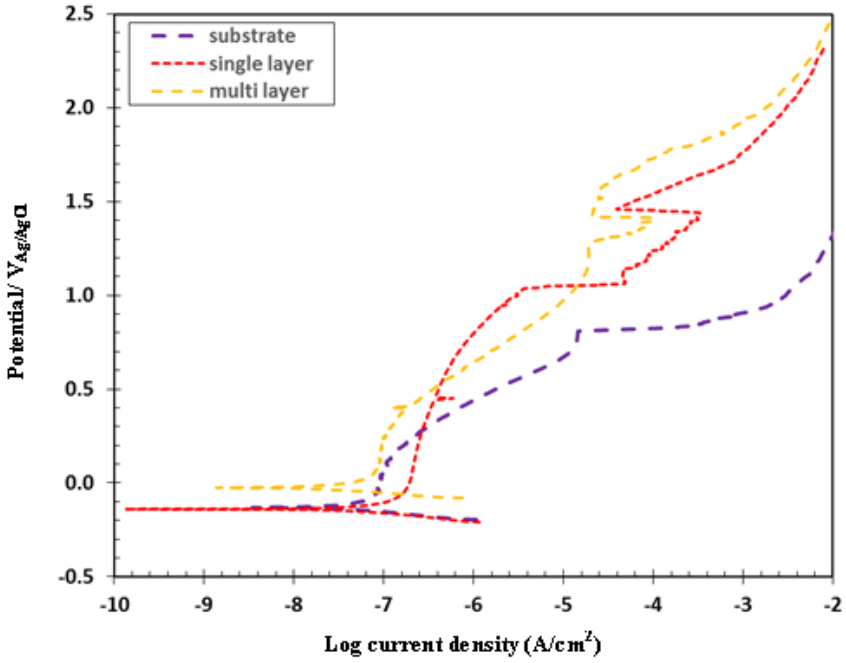

Fig. 10. Potentiodynamic polarization plots of 316L, TiN and Ti/TiN coatings in SBF solution for 336 h immersion

Fig. 11 reveals the SEM images of 316L, TiN and Ti/TiN coatings after 14 days immersion in SBF solution and potentiodynamic polarization test. Considering these images, the presence of pinholes arising from the corrosion in the single layer coating and 316L is visible and the surface of the multilayer coating is free of pinholes and serious damage and only a few small pinholes are visible on the surface. Fig. 12 depicts the obtained diagrams from EDS analysis of 316L, TiN and Ti/TiN coatings after 336 h immersion in SBF solution and polarization test. Table 6 summarizes the obtained data from Fig. 12. Based on the Fig. 12 and Table 6, calcium and phosphorus are also observed in addition to titanium and nitrogen on the surface of all three specimens. It can be said that the presence of these calcium phosphate compounds can probably amend the corrosion resistance by filling defects and surface pinholes and improving the surface pinholes.

Table 5. Extracted results from potentiodynamic polarization test after 336 h immersion in SBF solution

sample	E_{corr} ($V_{Ag/AgCl}$)	i_{corr} ($nA.cm^{-2}$)	E_b ($V_{Ag/AgCl}$)
316L	0.148	108	0.745
TiN	-0.164	170	0.979
Ti/TiN	-0.046	87	1.180

Table 6. Extracted results from EDS test after 336 h immersion in SBF solution

Sample	**Element**	**Weight Percent**	**Atomic Percent**
316L	Fe	69.61	66.04
	Cr	16.74	17.05
	Ni	9.9	8.93
	Mn	1.62	1.56
	O	1.77	5.86
	P	0.19	0.33
	Ca	0.18	0.23
TiN	N	22.25	39.83
	Ti	57.95	30.33
	Ca	0.1	0.06
	P	0.12	1.15
	O	18.28	28.63
Ti/TiN	N	18.62	34.3
	Ti	60.38	32.52
	Ca	0.38	0.24
	P	0.41	0.34
	O	20.21	32.59

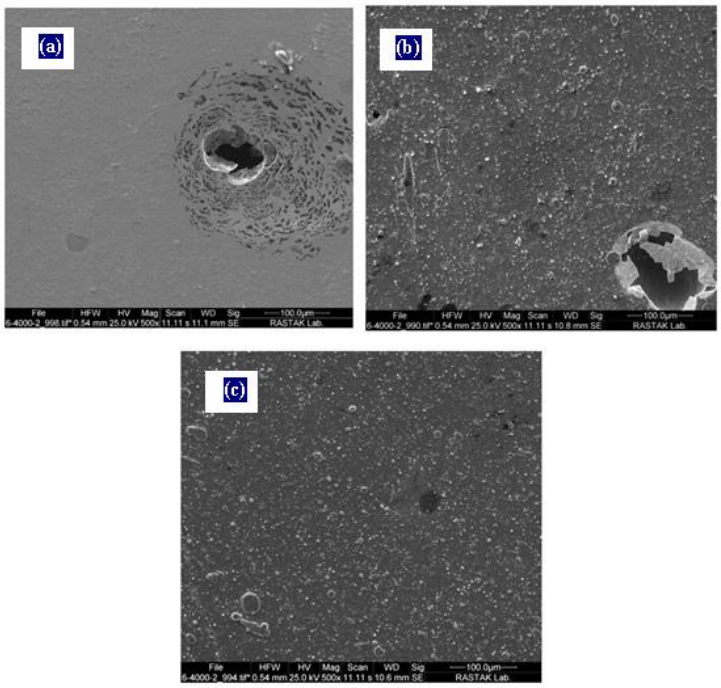

Fig. 11. SEM images of (a) 316L, (b) TiN single layer coating, and (c) Ti/TiN multilayer nanostructured coating samples after potentiodynamic polarization test in SBF solution (immersion time=336 h)

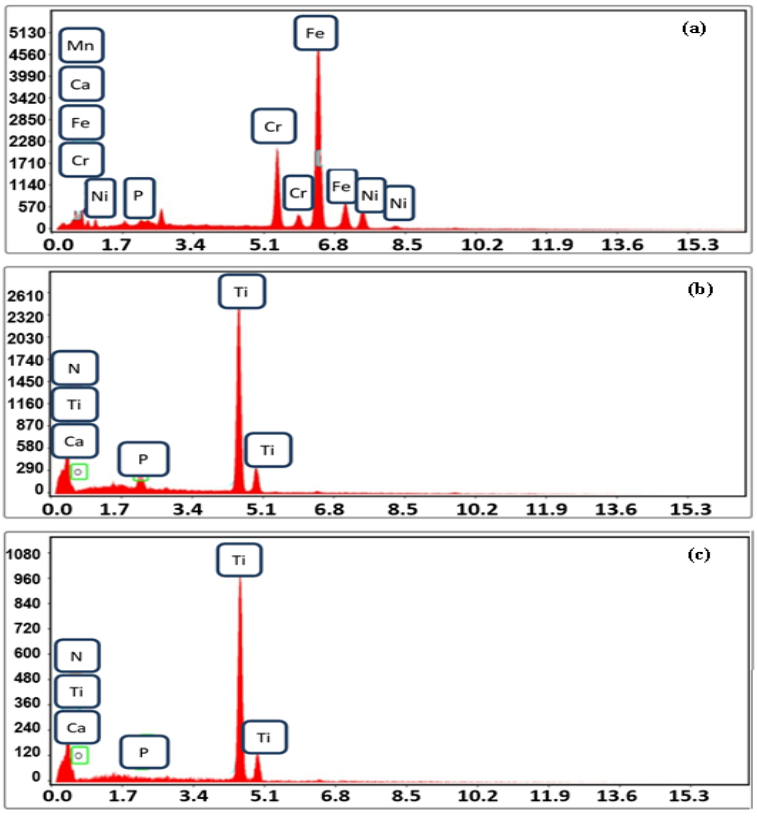

Fig. 12. Obtained diagrams from EDS of (a) 316L, (b) TiN single layer coating, (c) Ti/TiN multilayer coating after 336 h immersion in SBF solution and polarization test

4. CONCLUSION

TiN single layer and nanostructured Ti/TiN multilayer coatings were successfully deposited on AISI 316L substrate using CAE method. Microstructural features and corrosion resistance of these coatings were compared with 316L substrate in the simulated body solution (SBF). According to the nanoindentation test, the hardness of the nanostructured Ti/TiN coating is higher than that of TiN single layer coating. Based on AFM results, the number of average roughness for Ti/TiN multilayer is lower than TiN single layer coating which results in a more uniform passive layer having higher protective properties. The EIS measurement shows higher polarization resistance for Ti/TiN multilayer coating than TiN single layer coating and uncoated specimen. Also, the potentiodynamic polarization test shows higher corrosion current density for Ti/TiN multilayer coating than TiN single layer coating and uncoated specimen.

REFERENCES

[1] Q. Chen, and G. A. Thouas, Mater. Sci. Eng. R 87 (2015) 1.
[2] Y. Okazaki, and E. Gotoh, Biomaterials 26 (2005) 11.
[3] A. A. Zierold, Arch. Surg. 9 (1924) 365.
[4] N. S. Manam, W. S. W. Harun, D. N. A. Shri, S. A. C. Ghani, T. Kurniawan, M. H. Ismail, and M. H. I. Ibrahim, J. Alloys Compd. 701 (2017) 698.
[5] C. Leyens, M. Peters, eds., Titanium and Titanium Alloys, Wiley (2003).
[6] H. K. Koerten, J. J. M. Onderwater, E. W. A. Koerten, F. P. Bernoski, and R. G. H. H. Nelissen, J. Biomed. Mater. Res. 54 (2001) 591.
[7] H. Elmkhah, A. Fattah-alhosseini, K. Babaei, A. Abdollah-Zadeh, and F. Mahboubi, J. Asian Ceram. Soc. 8 (2020) 72.
[8] B. Podgornik, B. Zajec, N. Bay, and J. Vižintin, Wear 270 (2011) 850.
[9] H. Elmkhah, A. Abdollah-zadeh, F. Mahboubi, A. R. S. Rouhaghdam, and A. Fattah-alhosseini, J. Alloys Compd. 711 (2017) 530.
[10] H. Elmkhah, F. Attarzadeh, A. Fattah-alhosseini, and K. H. Kim, J. Alloys Compd. 735 (2018) 422.
[11] N. S. Mansoor, A. Fattah-alhosseini, H. Elmkhah, and A. Shishehian, Mater. Res. Express. 6 (2020) 126433.
[12] S. A. Naghibi, K. Raeissi, and M. H. Fathi, Mater. Chem. Phys. 148 (2014) 614.
[13] A. Fattah-alhosseini, H. Elmkhah, G. Ansari, F. Attarzadeh, and O. Imantalab, J. Alloys Compd. 739 (2018) 918.
[14] A. Fattah-alhosseini, H. Elmkhah, K. Babaei, O. Imantalab, H. R. Ghomi, and M. K. Keshavarz, Mater. Res. Express. 5 (2018) 106401.
[15] D. M. Mattox, Handbook of Physical Vapor Deposition (PVD) Processing, Elsevier,

2010.
[16] S. Arango, A. Peláez-Vargas, and C. García, Coatings 3 (2012) 1.
[17] P. Mohamadian Samim, A. Fattah-alhosseini, H. Elmkhah, and O. Imantalab, Mater. Res. Express. 6 (2019) 126426.
[18] Z. Andalibi Fazela, H. Elmkhaha, A. Fattah-alhosseinia, K. Babaeia and M. Meghdari, J. Asian Ceram. Soc. 8 (2020) 510.
[19] A. Gilewicz, P. Chmielewska, D. Murzynski, E. Dobruchowska, and B. Warcholinski, Surf. Coatings Technol. 299 (2016) 7.
[20] K. Jokar, H. Elmkhah, A. Fattah-alhosseini, K. Babaei, and A. Zolriasatein, Mater. Res. Express. 6 (2019) 116426.
[21] G. M. Pharr, D. L. Callahan, S. D. McAdams, T. Y. Tsui, S. Anders, A. Anders, J. W. Ager, I. G. Brown, C. S. Bhatia, S. R. P. Silva, and J. Robertson, Appl. Phys. Lett. 68 (1996) 779
[22] A. H. Tan, and Y. C. Cheng, Diam. Relat. Mater. 17 (2008) 36
[23] N. Sahib Mansoor, A. Fattah-alhosseini, A. Shishehian, and H. Elmkahah, Mater. Res. Express. 6 (2019) 056421.
[24] F. R. Attarzadeh, H. Elmkhah, and A. Fattah-alhosseini, Metall. Mater. Trans. B. 48 (2017) 227.
[25] A. Fattah-alhosseini, H. Elmkhah, and F. R. Attarzadeh, J. Mater. Eng. Perform. 26 (2017) 1792.
[26] L. Chenglong, Y. Dazhi, L. Guoqiang, and Q. Min, Mater. Lett. 59 (2005) 3813.
[27] N. D. Nam, M. J. Kim, D. S. Jo, J. G. Kim, and D. H. Yoon, Thin Solid Films. 545 (2013) 380.
[28] T. Kokubo, and H. Takadama, Biomaterials 27 (2006) 2907.
[29] A. K. Krella, Surf. Coatings Technol. 228 (2013) 115.
[30] B. Subramanian, R. Ananthakumar, and M. Jayachandran, Surf. Coatings Technol. 205 (2011) 3485.
[31] C. Liu, G. Lin, D. Yang, and M. Qi, Surf. Coatings Technol. 200 (2006) 4011.
[32] Q. Yang, D. Y. Seo, and L. R. Zhao, Surf. Coatings Technol. 177 (2004) 204.
[33] H. A. Jehn, Surf. Coatings Technol. 125 (2000) 212.
[34] C. Liu, P. K. Chu, G. Lin, and D. Yang, Corros. Sci. 49 (2007) 3783.
[35] W. Yanfeng, L. Zhengxian, W. Haonan, D. Jihong, and Z. Changwei, Rare Met. Mater. Eng. 46 (2017) 1219.
[36] Q. Wang, F. Zhou, C. Wang, M.-F. Yuen, M. Wang, T. Qian, M. Matsumoto, and J. Yan, Mater. Chem. Phys. 158 (2015) 74.
[37] W. Cui, G. Qin, J. Duan, and H. Wang, Mater. Sci. Eng. C 71 (2017) 520.
[38] B. Juttner, IEEE Trans. Plasma Sci. 15 (1987) 474.
[39] R. Ananthakumar, B. Subramanian, A. Kobayashi, and M. Jayachandran, Ceram. Int.

38 (2012) 477.

[40] H. C. Barshilia, M. S. Prakash, A. Poojari, and K. S. Rajam, Thin Solid Films. 460 (2004) 133.

[41] L. A. S. Ries, D. S. Azambuja, and I. J. R. Baumvol, Surf. Coatings Technol. 89 (1997) 114.

[42] R. A. Antunes, A. C. D. Rodas, N. B. Lima, O. Z. Higa, and I. Costa, Surf. Coatings Technol. 205 (2010) 2074.

[43] R. Ali, M. Sebastiani, and E. Bemporad, Mater. Des. 75 (2015) 47.

[44] N. Sahib Mansoor, A. Fattah-alhosseini, A. Shishehian, and H. Elmkhah, Anal. Bioanal. Electrochem. 11 (2019) 304.

[45] P. Mohamadian Samim, A. Fattah-alhosseini, H. Elmkhah, and O. Imantalab, J. Asian Ceram. Soc. 8 (2020) 460.

[46] N. Sahib Mansoor, A. Fattah-alhosseini, H. Elmkhah, and A. Shishehian, J. Asian Ceram. Soc. (2020) https://doi.org/10.1080/21870764.2020.1776915

[47] Z. W. Zhao, B. K. Tay, L. Huang, S. P. Lau, and J. X. Gao, Opt. Mater. (Amst). 27 (2004) 465.